Journal of Catalysis 352 (2017) 452–465

Contents lists available at ScienceDirect

Journal of Catalysis

journal homepage: www.elsevier.com/locate/jcat

Is water more reactive than H_2 in photocatalytic CO_2 conversion into fuels using semiconductor catalysts under high reaction pressures?

Hongwei Zhang [a], Shogo Kawamura [a], Masayuki Tamba [b], Takashi Kojima [b], Mao Yoshiba [a], Yasuo Izumi [a,*]

[a] Department of Chemistry, Graduate School of Science, Chiba University, Yayoi 1-33, Inage-ku, Chiba 263-8522, Japan
[b] Department of Applied Chemistry and Biotechnology, Graduate School of Engineering, Chiba University, Yayoi 1-33, Inage-ku, Chiba 263-8522, Japan

ARTICLE INFO

Article history:
Received 3 May 2017
Revised 10 June 2017
Accepted 12 June 2017

Keywords:
CO_2
Methane
Oxygen vacancy
Hydroxy group
TiO_2
Photocatalysis
Pressure dependence
Site separation
EXAFS
FTIR

ABSTRACT

The reaction pressure in the photocatalytic conversion of CO_2 into fuels is optimized between 0 and 0.80 MPa under CO_2 and moisture. The higher reactivity of water than H_2 was observed at higher pressure and the reason was clarified using several ~10-μm-thick semiconductor-based photocatalysts. The best Pd/TiO_2 photocatalyst produces methane with a reaction order of 0.39. The sum of independent total formation rates of C-containing compounds under UV and visible light does not account for that under UV–visible light, demonstrating synergetic reaction mechanism on Pd for CO_2 reduction by excited electrons via surface plasmon resonance and on TiO_2 for water oxidation. Active metallic Pd and O vacancy sites due to O_2 formation from H_2O are confirmed by in situ monitoring of EXAFS [N(Pd–Pd) = 5.9–6.2; N(Ti–O) = 5.2–3.5] and the decrease of the H-bound and bi/tri-coordinated OH peaks in FTIR. Effective redox-site separation explains the higher reactivity of water than H_2.

1. Introduction

Photocatalytic conversion of CO_2 into fuels is one of the routes to producing carbon neutral fuels without a net increase in atmospheric CO_2 concentrations associated with fossil-derived alternatives [1–3]. TiO_2 has been investigated most intensively for this purpose and produces methane and/or CO [1–3]. The CO_2 conversion reaction includes two steps: water oxidation, utilizing natural light similar to Photosystem II (Eq. (1)) [4], followed by CO_2 photoconversion using a photocatalyst to form methane (Eq. (2)), CO, methanol, formic acid, and formate ions [5–15] similar to Photosystem I, in which a strong reductant is formed capable of reducing nicotinamide adenine dinucleotide phosphate ($NADP^+$) to NADPH [4].

$$2H_2O(g) \rightarrow O_2(g) + 4H^+(\text{surface}) + 4e^- \quad (1)$$

$$CO_2(g) + 8H^+(\text{surface}) + 8e^- \rightarrow CH_4(g) + 2H_2O(g) \quad (2)$$

Recently, studies of CO_2 photoreduction, using CO_2 and H_2, including a reduction step (Eq. (2)) were reported under a reaction pressure up to 0.80 MPa [16,17]. The CO_2 photoreduction rates followed the order

$$Pd/TiO_2 > Cu/TiO_2 >> Ag/ZrO_2 \sim \text{graphitic} - C_3N_4 > Ag/[Zn_3Ga(OH)_8]_2CO_3 \cdot mH_2O \sim BiOCl \quad (3)$$

as a function of the potential of hot/excited electrons and charge separation efficiency for the semiconductors [16]. The best Pd/TiO_2 catalyst exclusively produced methane on Pd, starting from CO_2, coupled with (a) hot electrons consecutively excited by the band-gap (BG) excitation of TiO_2 and surface plasmon resonance (SPR) [18] on Pd and (b) protons formed from H_2 at the interface with the TiO_2 surface.

Studies on the CO_2 photoreduction into methanol were also reported using H_2 and various layered double hydroxides (LDHs) photocatalysts [19–21]. Furthermore, the reduction step (Eq. (2)) and oxidation step (Eq. (1)) were combined using LDH and WO_3, respectively, in tandem cell separated by a proton-conducting film [22].

For the CO_2 photoconversion with water, on the oxidation reaction side (Eq. (1)), water/surface hydroxy activation by hole to form a hydroxy radial (·OH) on TiO_2 has been widely suggested [7].

* Corresponding author.
E-mail addresses: zhw9590@yahoo.co.jp (H. Zhang), dan556.1020@gmail.com (S. Kawamura), affa3553@chiba-u.jp (M. Tamba), tkojima@faculty.chiba-u.jp (T. Kojima), yubari.com@ae.auone-net.jp (M. Yoshiba), yizumi@faculty.chiba-u.jp (Y. Izumi).

http://dx.doi.org/10.1016/j.jcat.2017.06.016
0021-9517/

$$H_2O(g) + h^+ \rightarrow {\cdot}OH + H^+(surface) \quad (4)$$

$$OH(surface) + h^+ \rightarrow {\cdot}OH \quad (4')$$

The highly reactive ·OH radical is closely related to O_2 formation and O vacancy (O_V) sites via

$${\cdot}OH + OH(surface) + 3h^+ \rightarrow O_2(g) + O_V + 2H^+(surface) \quad (5)$$

$${\cdot}OH + O(surface) + 3h^+ \rightarrow O_2(g) + O_V + H^+(surface) \quad (5')$$

Furthermore, CO_2 conversion into CO on O_V sites on TiO_2 is also recently suggested experimentally [5–8] and theoretically [23,24] via Eqs. (6) and/or (7) and (8).

$$CO_2(g) + O_V \rightarrow CO(g) + O(surface) \quad (6)$$

$$CO_2(g) + Ti^{3+} \rightarrow Ti^{4+} - CO_2^- \quad (7)$$

$$Ti^{4+} - CO_2^- + H^+(surface) + e^- \rightarrow CO(g) + OH^-(surface) \quad (8)$$

The photoconversion of CO_2 was accelerated at an elevated reaction pressure of CO_2 and moisture [5,6] or liquid water [6,9–12,25,26]. The formation rates of CO and methane on TiO_2 were higher using moisture (12.3 kPa) rather than liquid water [6]. The pressure dependence has not been systematically reported using CO_2 and water/moisture in comparison to systematic studies on CO_2 photoreduction using CO_2 and H_2 at a reaction pressure of 0.10–0.80 MPa that showed volcano-type dependence [16]. Therefore, in this study, we systematically optimize CO_2 photoconversion using moisture and Pd/TiO_2 photocatalyst based on the investigations of catalyst optimization, pressure dependence, and reaction mechanism. As a result, moisture is more reactive than H_2 for CO_2 photoconversion under the reaction conditions in this study, contrary to the order of standard reduction potential for H_2 [$E°$@298.15 K versus standard hydrogen electrode (SHE), pH 0] (Eqs. (9) and (10)). The order predicts that H_2 at a high potential provides electrons more easily.

$$2H^+(surface) + 2e^- \rightarrow H_2(g), E° = 0\ V \quad (9)$$

$$O_2(g) + 4H^+(surface) + 4e^- \rightarrow 2H_2O(g), E° = 1.229\ V \quad (10)$$

The reason for the higher reactivity of water in comparison to H_2 under the conditions in this study is successfully explained for the first time using X-ray absorption fine structure (XAFS) and Fourier-transform infrared (FTIR) spectroscopy, and the mass balance in kinetic tests under various reaction conditions. To check and confirm an advantage of the combination of CO_2 and water on spacially segregated redox surface sites as compared to that of CO_2 and H_2, Pd/TiO_2 photocatalyst was tested that was already used and proved to be the best for the studies under CO_2 and H_2 [16].

2. Experimental

2.1. Catalyst synthesis/preparation

The synthesis/preparation procedure of catalysts used in this study (Table 1) was described in our preceding paper [16]. Supported Pd catalyst on TiO_2 was prepared via liquid-phase reduction starting from 1.0 mM of Na tetrachloropalladate (>98%, Sigma Aldrich) and TiO_2 (P25, Degussa; anatase:rutile phase = 4:1, specific surface area 60 $m^2\ g^{-1}$) stirred at 290 K for 24 h. Then, 40 mM of $NaBH_4$ aqueous solution was added in a molar ratio of Pd: $NaBH_4$ = 1:8 and the suspension was stirred at 290 K for 1 h, filtered, and the obtained gray precipitate was washed with deionized water before drying under vacuum at 290 K for 24 h. The obtained catalyst was denoted as Pd/TiO_2 and the Pd content was 0.5 wt% (Table 1).

2.2. Characterization

Cross-sectional scanning electron microscopy (SEM) images were obtained using a model JSM-6510 (JEOL). A tungsten filament was used in the electron gun, and the electron accelerating voltage was 20 kV. The photocatalyst film formed on a Pyrex glass plate was cut and mounted on the Al sample holder using an adhesive. The incident angle of electrons with a reference to the normal line of the sample surface was between 75° and 85°. The magnification was between 200 and 3000 times. High-resolution transmission electron microscopy (HR-TEM) images were observed using a Model H-7650 transmission electron microscope (Hitachi) at an accelerating voltage of 100 kV. A tungsten filament was used in the electron gun and the samples were mounted on conducting carbon with a Cu grid mesh (150 mesh per inch). The magnification was between 60,000 and 200,000 times.

X-ray diffraction (XRD) patterns were measured using a model Mini Flex (Rigaku) at a Bragg angle (θ_B) of $2\theta_B$ = 20–60° with a scan step of 0.02° and a scan rate of 0.3 s per step. The data scan was performed at 30 kV and 15 mA using Cu Kα emission (wavelength λ = 0.15419 nm) [27] and a nickel filter. Crystallite sizes (t) were estimated using the Scherrer equation

$$t = \frac{0.9\lambda}{\text{Peak width} \times cos\theta_B}. \quad (11)$$

Palladium K-edge XAFS spectra were measured at 290 K in the transmission mode in the Photon Factory Advanced Ring at the High Energy Accelerator Research Organization (KEK, Tsukuba) on beamline NW10A [28,29]. The storage ring energy was 6.5 GeV, and the ring current was 52.1–20.7 mA. A Si (3 1 1) double-crystal monochromator and a Pt-coated focusing cylindrical mirror were inserted into the X-ray beam path. The X-ray intensity was maintained at 67% of the maximum flux using a piezo-translator applied to the crystal to suppress higher harmonics. The slit in front of the I_0 ionization chamber had an opening size of 1 mm (vertical) × 2 mm (horizontal). Separately, during the photoconversion tests, the samples (10 mg) on the Pyrex glass plates were placed under 0.40 MPa CO_2 and 2.3 kPa of moisture, and measurements took place at 290 K in the fluorescence mode using a Lytle detector, placing 3-μm-thick RuO_2 filter between the sample and the I_f ion chamber [30]. The Pd K-edge absorption energy was calibrated to 24,348 eV using the spectrum of a 12.5-μm-thick Pd foil [27].

Titanium K-edge XAFS spectra were measured in the KEK Photon Factory on beamline 9A, 9C, and 12C [31]. The storage ring energy was 2.5 GeV, and the ring current was 449.3–324.4 mA. A

Table 1
Basic physicochemical properties of Pd/TiO_2 photocatalyst used for tests under CO_2 and moisture in this study.

Pd loading (wt%)	Color	Pd mean particle size (nm)		TiO_2 mean particle size (nm)	
		TEM	EXAFS	HR-TEM	XRD
0.5	Gray	3.1 [16]	1.1(± 0.1) {2.6(± 0.3)[*1]}	30–50 [16]	25(± 8) [16]

[*1]After photocatalytic tests under CO_2 (3.4 kPa) + moisture (1.2 kPa) for 5 h.

Si (1 1 1) double-crystal monochromator and a pair of bent conical/cylinder mirrors and/or double flat mirrors were inserted into the X-ray beam path. Spectra for the Pd/TiO_2 sample (10 mg) diluted by boron nitride were measured in the presence/absence of ultraviolet (UV)–visible irradiation provided by a 500-W Xe arc lamp (model OPM2-502, Ushio) at the beamline [32]. The Ti K-edge absorption energy was calibrated to 4964.5 eV using the spectrum of the 5-μm-thick Ti foil [27].

XAFS data were analyzed using the XDAP software package [33]. The pre-edge background was approximated by a modified Victoreen function $C_2/E^2 + C_1/E + C_0$. The background of the post-edge oscillation was approximated by a smoothing spline function and was calculated using Eq. (12) for the particular number of data points i, where k was the angular wavenumber of photoelectrons, μ was the X-ray absorption coefficient, t was the thickness of sample, and the typical values for smoothing factor were between 0.1 and 3.

$$\sum_{i=1}^{\text{Data Points}} \frac{(\mu t_i - \text{Background}_i)^2}{\exp(-0.075k_i^2)} \leqslant \text{smoothing factor} \tag{12}$$

Multiple-shell curve fitting was performed [16,31] for the Fourier-filtered k^3-weighted extended XAFS (EXAFS) data in k- and interatomic distance (R)-space using empirical amplitudes extracted from the EXAFS data for Pd foil, PdO powder, and rutile-type TiO_2 powder. The R and its associated coordination number (N) for the Pd–Pd, Pd–O, Ti–O, and Ti(–O–)Ti pairs were set to 0.275 09 nm with an N value of 12 [34], 0.2026 nm with an N value of 4 [35], 0.1959 nm with an N value of 6, and 0.3058 nm with an N value of 12 [31,36,37], respectively. The many-body reduction factor S_0^2 was assumed to be equal for both the sample and the reference.

The number of independent data points (ν) in the fit range was calculated based on the Nyquist theorem modified for EXAFS by Stern based on the ranges of k and R [33].

$$\nu = \frac{2\Delta k \Delta R}{\pi} + 2 \tag{13}$$

Based on the fitting and error analysis presented in our previous paper [16], two shell fits (four variables in each shell) were chosen for both Pd and Ti K-edge EXAFS analyses.

The adsorption of O_2 was monitored for 100 mg Pd/TiO_2 fine powder that was previously irradiated using UV–visible light for 5 h in a quartz glass reactor connected to a Pyrex glass system under vacuum connected to rotary and diffusion pumps (10^{-6} Pa) [2]. Then, 2.3 kPa of O_2 was introduced to the glass system and the pressure change was monitored using a capacitance manometer (models CCMT-100A and GM-2001, ULVAC) under the irradiation of UV–visible light for 1 h and then in the absence of light for 5 h. The temperature was 295 K and the total volume of the glass system was 167.4 mL.

FTIR spectra were measured using a model FT/IR-4200 spectrophotometer equipped with a mercury-cadmium-tellurium-M detector (JASCO) in the wavenumber region between 4000 and 650 cm^{-1}. 100 mg of the photocatalyst disk was set on a holder in a quartz cell equipped with two NaCl windows on both sides and connected to a glass system that could be evacuated using rotary and diffusion pumps (10^{-6} Pa) [32].

Separately, the quartz cell was connected to the glass system, but 100 mg of the Pd/TiO_2 powder was placed in quartz glass reactor connected to the glass system. The photocatalyst was irradiated by UV–visible light from Xe arc lamp and the changes of reaction gases [CO_2 and moisture, $^{13}CO_2$ (purity > 99.5%, ^{13}C 99%, Cambridge Isotope Laboratories) and moisture] was monitored by FTIR.

2.3. High-pressure photoconversion tests of CO_2

The synthesized/prepared catalysts (Table 1) were immersed in deionized water and agitated by ultrasound (430 W, 38 kHz) for 3 min. The suspension was mounted on a Pyrex glass plate (25 mm × 25 mm × 1 mm) and dried at 373 K for 12 h. The area of the obtained film was 20 mm × 20 mm. The films on the plates or the as-synthesized fine powder samples in Pyrex dishes (Φ_{internal} = 37 mm) were introduced into a homemade high-pressure stainless steel reactor equipped with quartz double windows, a pressure gauge, and Swagelok valves [16,17]. The effective internal volume of the reactor was 98.4 mL.

CO_2 gas (0.12–0.80 MPa) was introduced through a stainless water bubbler (Taiatsu Glass Kogyo, inner volume 120 mL; model TVS-N2-120) at 293 K. The photocatalyst in the stainless steel reactor was irradiated with UV–visible light provided by a 500-W Xe arc lamp (model OPM2-502, Ushio) through the quartz windows for 5 h. The distance between the light exit and the photocatalyst surface was 82.7 mm, and the light intensity at the center of the photocatalyst was 81.6 mW cm^{-2} [16]. The quartz window of the high-pressure reactor absorbed/reflected 9.5% of the light, and 100 mg of Pd/TiO_2 powder on Pyrex dish and 10 mg Pd/TiO_2 film on Pyrex glass plate absorbed/reflected/scattered 40% and 49% of the light, respectively [16]. Densely mounted films were advantageous for light absorption efficiency compared with fine Pd/TiO_2 powders based on the difference of their mean area densities of 2.5 mg cm^{-2} and 9.3 mg cm^{-2}, respectively, and the exposed ratio of particles. Fine powders should reflect/scatter more light at exposed faces, and less light reach the lower part of the layers compared to densely mounted films.

For comparison, photocatalytic tests were also performed using L37, L38, L39, L42, Y48, and Y52 filters (2.5 mm-thick, Kenko) that removes light less than λ = 370, 380, 390, 420, 480, and 520 nm, respectively [38], or a U-330 filter (2.5 mm-thick, Kenko) that removes light less than λ = 250 nm and between λ = 390 nm and 695 nm [39], which were set between the light exit and high-pressure reactor.

After irradiation for five hours, the reaction gas was analyzed using packed columns of 13X-S molecular sieves and polyethylene glycol (PEG-6000) supported on a Flusin P (GL Sciences) set in a gas chromatograph (GC) equipped with a thermal conductivity detector (model GC-8A, Shimadzu) [19,20]. Helium (>99.999 95%) was used as a carrier gas for all analytes except H_2, for which argon (>99.998%) was used instead. The amount of methanol and moisture was double-checked by concentrating them using a trap made of a mixture of diethyl ether and dry ice (192 K) [17] in order to separate them from H_2 and most of CO_2.

Blank tests were also performed by eliminating one of the four control factors or adding an alternative control factor: (i) *reactants*, (ii) *catalyst*, (iii) *UV–visible light*, and (iv) *temperature*, i.e., in 0.40 MPa of CO_2 only, in 2.3 kPa moisture only, or 0.4 MPa He or Ar (in the absence of any reactants), in the absence of catalyst (or in the absence of Pd or O_V sites), in the absence of any light at 299 K or 353 K, in the absence of UV light at 296 K, and in the absence of (most of) visible light at 296 K.

3. Results

3.1. Cross-sectional SEM, HR-TEM, and XRD observation of films

The surface of the fresh Pd/TiO_2 film (Fig. 1a1, a2) [16] and the one used for photoconversion test under CO_2 (0.40 MPa) and moisture (2.3 kPa) for 5 h (Fig. 1b1, b2) both on Pyrex glass are flat and smooth within the variance of 5 μm, based on cross-sectional SEM images. In the close-ups (Fig. 1a2, b2), the mean film thickness is 14 μm ± 3 μm. In the comparison between fresh and used samples,

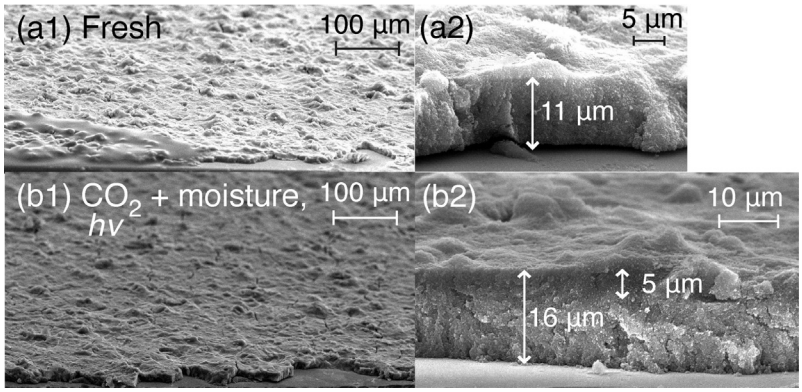

Fig. 1. Cross-sectional SEM images of Pd/TiO_2, fresh (a1, a2) [16] and after CO_2 photoreduction testing, under CO_2 (0.40 MPa) and moisture (2.3 kPa) for 5 h (b1, b2). (a1, b1) show wide views, and (a2, b2) show close-ups.

the homogeneous light gray contrast in the fresh sample (Fig. 1a1, a2) changes to more densely packed dark gray from the surface (b1) until the upper approximately 5 μm of the film (b2). Such change is observed in more than the half of the cross-sectional views for used samples, suggesting partial reduction of the upper TiO_2 layer to include more O_V sites (Eqs. (5) and (5′)). To confirm the crystalline phase, the XRD pattern is measured for these samples. The peak intensity and the width for anatase 1 0 1, 1 0 3, 1 1 2, 2 0 0, 1 0 5, and 2 1 1 and rutile 1 1 0, 1 0 1, and 0 0 4 diffraction does not change significantly (by 4–10% and 13–19%, respectively, except for very weak peaks) after the photoconversion test (Supplementary material, Fig. S1 and Table S1). The mean particle size is evaluated at 25 ± 8 nm based on Eq. (11) for eight peaks [16] (Table 1). The anatase 1 0 1 peak of low surface energy is relatively weaker for the films compared to that for fine powder, suggesting higher surface energy in the exposed crystalline face of the films [16]. The mean particle size was in accordance with the distribution obtained based on HR-TEM (30–50 nm, Table 1) if lower detection limit for TEM (~0.2 nm) is taken into account.

3.2. Monitoring the active sites using Pd and Ti K-edge XAFS

The Pd states are monitored by Pd K-edge X-ray absorption near-edge structure (XANES). The post-edge pattern for fresh Pd/TiO_2 sample (Fig. 2c) is not the same as that for PdO or Pd foil (a, b) but mostly resembles that for the mixture of spectra for Pd foil and PdO with the mixing ratio 3:2 (f; see also the comparison in Fig. 2, right, top).

Then, 100 mg of Pd/TiO_2 is placed under CO_2 (3.4 kPa) and moisture (1.2 kPa) and UV–visible light for 5 h (Table 3A-a). The XANES post-edge pattern (Fig. 2d) resembles more that of the mixture of spectra for Pd foil and PdO with the mixing ratio 3:1 (Fig. 2g; see also the comparison in Fig. 2, right, bottom). Conversely, the post-edge pattern for 10 mg Pd/TiO_2 under higher CO_2 pressure (0.40 MPa) and moisture (2.3 kPa) and UV–visible light for 5 h (Table 3A-d) resembles more that of fresh Pd/TiO_2 (Fig. 2c, e). Following, the sample of Fig. 2e is irradiated under UV–visible light during XANES measurement (Fig. 2e′). The intensity of the first post-edge peak at 24,370 eV becomes weaker, suggesting a decrease in the O-coordination around the Pd site.

As a complement to XANES, under CO_2 (3.4 kPa) and moisture (1.2 kPa) and UV–visible light for 5 h (Table 3A-a), the *N* value for the Pd–Pd interatomic pair based on EXAFS analysis is 9.2 (Table 2A-d), corresponding to a mean particle size of 2.6(±0.3) nm (Table 1) [40]. Accordingly, the Pd–Pd interatomic pair is more pronounced in the Fourier transform (Fig. S2A-d), in consistency with the XANES pattern with greater Pd^0 contribution (Pd^0: Pd^{II} = 3:1; Fig. 2d). Conversely, the *N*(Pd–Pd) value changes negligibly from fresh Pd/TiO_2 (5.9) to that after 0.40 MPa of photoconversion test for 5 h (6.2; Table 2A-c, e), demonstrating

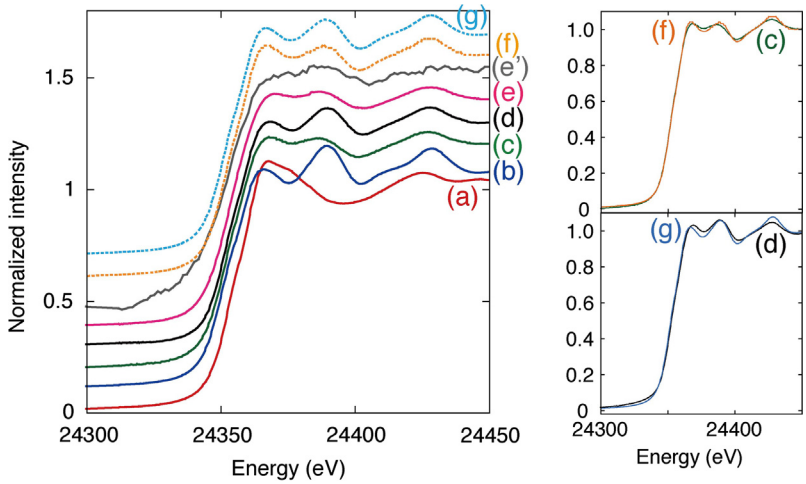

Fig. 2. Pd K-edge XANES for PdO (a), Pd foil (b), Pd/TiO_2 photocatalyst (100 mg; fresh) (c), under CO_2 (3.4 kPa) and moisture (1.2 kPa) for 5 h irradiated by UV–visible light (d), under CO_2 (0.40 MPa) and moisture (2.3 kPa) for 5 h irradiated by UV–visible light (e), Pd/TiO_2 (10 mg) after the condition of spectrum e was irradiated by UV–visible light during XAFS measurement (e′), and the mixture of spectra a and b with the mixing ratio of 3:2 (f) and 3:1 (g). The spectra were obtained in the transmission mode, except for Pd K-edge for samples e′, which were taken in the fluorescence mode. (*Right two panels*) Good agreements between spectra c and f (*Top*) and between spectra d and g (*Bottom*).

Table 2
Best-fit results of (A) Pd K-edge and (B) Ti K-edge EXAFS spectra for TiO_2 and Pd/TiO_2 photocatalysts.

Entry	Samples	Pd–O R (nm) N $\Delta(\sigma^2)$ (10^{-5} nm^2)	Pd–Pd R (nm) N $\Delta(\sigma^2)$ (10^{-5} nm^2)	Goodness of fit
(A)				
c [16]	Pd/TiO_2, fresh, 100 mg	0.199 (±0.006) 1.9 (±0.4) −4.8 (±1.7)	0.276 (±0.001) 5.9 (±0.5) 5.0 (±0.6)	1.2×10^3
d[*1]	5-h photocatalytic test under CO_2 (3.4 kPa) + moisture (1.2 kPa), 100 mg	0.216 (±0.009) 0.8 (±0.2) 0.2 (±0.2)	0.2753 (±0.0003) 9.2 (±0.3) 3.0 (±0.3)	3.9×10^2
e[*2]	5-h photocatalytic test under CO_2 (0.40 MPa) + moisture (2.3 kPa), 100 mg	0.201 (±0.001) 1.0 (±0.3) −2.6 (±1.3)	0.2765 (±0.0001) 6.2 (±0.5) 3.6 (±0.4)	1.0×10^3
(B)				
Entry	Samples	Ti–O R (nm) N $\Delta(\sigma^2)$ (10^{-5} nm^2)	Ti(–O–)Ti R (nm) N $\Delta(\sigma^2)$ (10^{-5} nm^2)	Goodness of fit
c-supp	TiO_2 (P25)	0.197 (±0.001) 6 (±2) 3 (±1)	0.312 (±0.02) 12 (±2) −1 (±1)	9.7×10^4
c	Pd/TiO_2, fresh, 10 mg	0.1989 (±0.0004) 5.4 (±0.1) 1.1 (±0.2)	0.3128 (±0.0002) 9.28 (±0.05) −3.5 (±0.1)	3.2×10^4
e[*3]	5-h photocatalytic test under CO_2 (0.40 MPa) + moisture (2.3 kPa), 10 mg	0.1989 (±0.0002) 5.2 (±0.3) −0.2 (±0.4)	0.31 (±0.01) 12 (±1) −2.4 (±0.7)	5.8×10^6
e′[*3,*4]	5-h photocatalytic test under CO_2 (0.40 MPa) + moisture (2.3 kPa), irradiated at beamline, 10 mg	0.2000 (±0.0002) 3.5 (±0.3) −1.7 (±0.5)	0.312 (±0.003) 10 (±3) −2 (±2)	5.5×10^6

[*1,*2] After photocatalytic test listed in Table 3A-a[*1] and A-b.[*2]
[*3] Similar conditions after photocatalytic test listed in Table 3A-d, but mixed with boron nitride.
[*4] The sample was irradiated by UV–visible light for 1 h during XAFS measurements at beamline.

Table 3
Dependence of CO_2 photoconversion using moisture on the amount of photocatalysts and reactant pressure and control test results in the absence of UV and/or visible light, catalyst, or reactant (A) and the comparisons to CO_2 photoconversion using H_2 [16] at the same total pressure of reactants (CO_2 and moisture versus CO_2 and H_2) (B).

Entry	Photocatalysts		Reactants (MPa)		Formation rates (μmol h^{-1} g_{cat}^{-1})						
	Type	Wt (mg)	CO_2	H_2O	CO	CH_3OH	CH_4	H_2	H_2O	O_2	$\sum_C^{*1}$
(A)											
a	Pd/TiO_2	100	0.0034	0.0012	<0.008	<0.0004	0.9	6.9	–	0.25	0.9
b			0.40	0.002 3	<0.008	0.002	1.4	17		0.36	1.4
c		10	0.12		<0.08	0.065	14	55		7.1	14
d			0.40		4.1	0.063	19	181		5.5	23
d′[*2]					<0.08	0.23	<0.12	<0.02		<0.08	0.23
d″[*3]					<0.08	0.047	7.4	42		1.2	7.4
d‴[*4]					<0.08	<0.004	<0.12	<0.02		<0.08	<0.20
d⁗[*5]					<0.08	<0.004	<0.12	<0.02		<0.08	<0.20
d⁗′[*6]			0	0	<0.08	<0.004	<0.12	<0.02	8.2	<0.08	<0.20
e			0.40[*7]	0[*7]	5.4	0.065	25	37	30	5.5	31
f[*6]			0	0.002 3	<0.08	<0.004	<0.12	106	–	18	<0.20
g			0.80		6.3	0.52	30	291		6.5	37
h	TiO_2		0.40		<0.08	<0.004	<0.12	6.7		<0.08	<0.20
h′[*8]					<0.08	<0.004	<0.12	4.2		<0.08	<0.20
i	*No catalyst*	0			<0.0008[*9]	<0.00004[*9]	<0.0012[*9]	<0.0002[*9]		<0.0008[*9]	<0.0020[*9]

(B) Using Pd/TiO_2 (10 mg)

Entry	(i) CO_2 Photoconversion under CO_2 and moisture		(ii) CO_2 Photoconversion under CO_2 and H_2[*10]			
	Reactants (MPa)	Formation rates (μmol h^{-1} g_{cat}^{-1})	Reactants (MPa)		Formation rates (μmol h^{-1} g_{cat}^{-1})	
	CO_2	H_2O	$\sum_C^{*1}$	CO_2	H_2	$\sum_C^{*1}$
d	0.40	0.002 3	23	0.12	0.28	38 (*faster*)
g	0.80		37 (*faster*)	0.24	0.56	8.6

[*1] Total molar amount of products comprising C. [*2,*3] Using L42 filter[*2] and U330 filter[*3] at the light exit. Temperature = 296 K. [*4,*5] In the absence of UV–visible light at 299 K[*4] and at 353 K. [*5,*6] In 0.40 MPa of helium or argon. [*7] Mixed gas of 0.10 MPa of CO_2 and 2.3 kPa of H_2O was flowed prior to the introduction of 0.40 MPa of CO_2. [*8] Catalyst was irradiated under UV–visible light for 4 h and vacuum prior to the test. [*9] In the unit of μmol h^{-1}. [*10] Results using CO_2 and H_2 were reported in Ref. [16].

that the Pd valence state and the mean particle size change only slightly under these conditions. In contrast, the N(Pd–O) value decreases from 1.9 for fresh to 1.0 after the test at 0.40 MPa, suggesting an increase of the O_V sites at the interface between the Pd and TiO_2 surfaces.

To complement the Pd K-edge results, Ti K-edge EXAFS is studied for Pd/TiO_2 (10 mg) as prepared (Table 2B-c and Fig. S2B-c) and after testing under 0.40 MPa CO_2, moisture, and UV–visible light irradiation for 5 h (Table 2B-e and Fig. S2B-e). The N(Ti–O) values are 5.4 and 5.2, respectively, smaller compared to 6 for untreated TiO_2 (Table 2B-c-supp), or 6.1 for the sample under 0.40 MPa CO_2 and H_2, and UV–visible light irradiation for 5 h [16], suggesting minor O_V site formation during liquid-phase reduction to prepare Pd/TiO_2 catalyst. Conversely, the decrease (0.2) under CO_2 and moisture and UV–visible light is insignificant, taking the fit errors (±0.1 to 0.3) into account.

Pd/TiO_2 after the test at 0.40 MPa for 5 h is irradiated by UV–visible light during the Ti K-edge EXAFS measurement at beamline (Table 2B-e′ and Fig. S2B-e′). The N(Ti–O) value decreases to 3.5, suggesting a dramatic increase of the number of O_V sites during UV–visible light irradiation. The O_V sites are reversibly filled by O species after the light is turned off, because the N(Ti–O) value increases to 5.2 in the absence of UV–visible light irradiation (Table 2B-c, e). During the irradiation of UV–visible light, the N(Ti–O) and $\Delta(\sigma^2)$ values may be difficult to determine exactly due to the fast reaction with the ·OH radical to form O_V sites on an ns or μs time scale [41]. Similar uncertainty of metal–O coordination is reported for BiOCl [N(Bi–O) = 4 → 1.9] [28].

Under CO_2 (100 kPa), moisture (2.2 kPa), and UV–visible light, the change in N(Ti–O) values was monitored (Fig. 3A, C). In comparison to the initial value (6.0) under CO_2, moisture, and dark, the value significantly decreased to 4.9–5.7 (mean value 5.3) during light irradiation for 3.5 h. At 30 min after the light was off, the N(Ti–O) value increased to the original value (6.0). N(Ti(–O–)Ti) values followed a similar trend: decrease from initial 11.3 to 9.7–10.6 during the irradiation of UV–visible light and increase to 10.9 at 30 min after the light was off (Fig. 3B). Taking the experimental and fit errors into account (Fig. 3A, B), the N(Ti–O) and N(Ti(–O–)Ti) values would evaluate the concentration of O_V sites in/on TiO_2 semi-quantitatively.

Corresponding to the time course of Ti K-edge EXAFS, that of Ti K pre-edge region was also plotted (Fig. 3D–F). In comparison to data for fresh sample under CO_2 (100 kPa), moisture (2.2 kPa), and dark (Fig. 3D: 0 min), the peak pattern changed after the UV–visible light was irradiated, especially in the region between 4968 and 4971 eV (Fig. 3D: 5, 30 min). This trend is in good agreement with the increase of pre-edge peak at 4967.6 eV owing to 5 coordination Ti sites [42–44] or 4 coordination Ti sites [43,44] in comparison to that at 4968.8 eV owing to 6 coordination Ti sites [42]. Please note that there is minor energy calibration difference between reference 42 and this study.

While the peak pattern negligibly changed during the UV–visible irradiation (Fig. 3E: 60, 100, 130, 150 min; Fig, 3F: 180 min), the pattern clearly changed after the light was off (Fig. 3F: light off 0, 30 min). The last two peak patterns were very similar to that of fresh sample before light irradiation (Fig. 3D: 0 min), in consistent

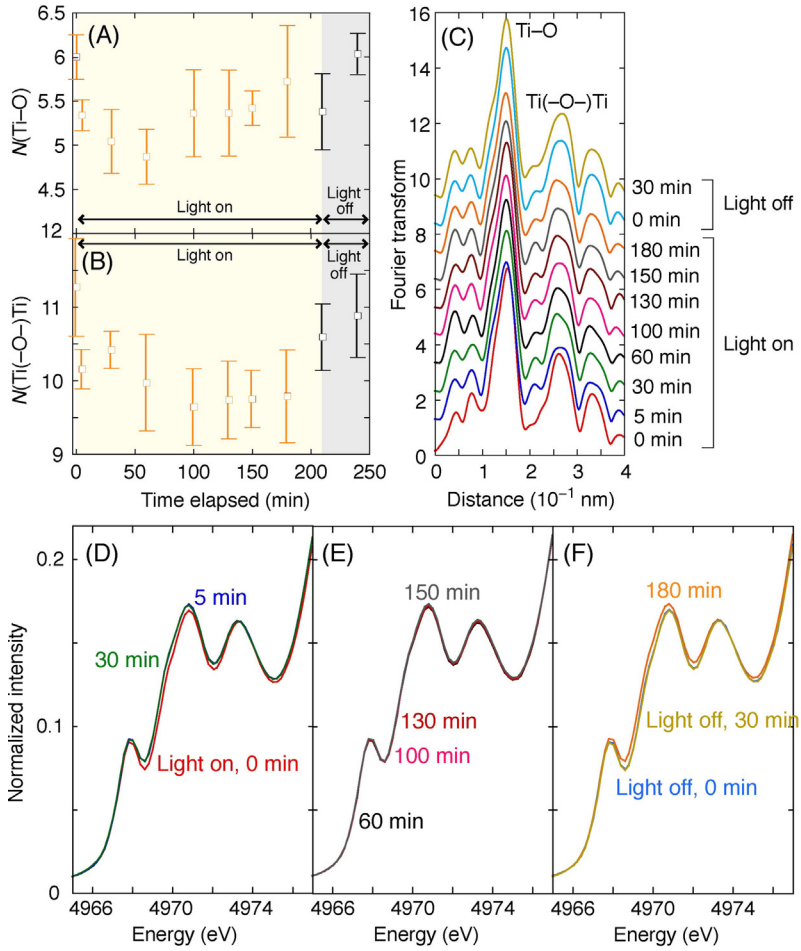

Fig. 3. Time course of Ti K-edge (A–C) EXAFS and (D–F) pre-edge region for Pd/TiO_2 photocatalyst (10 mg) under CO_2 (100 kPa) and moisture (2.2 kPa) for 3.5 h irradiated by UV–visible light and subsequently for 0.5 h under dark. The changes of (A) N(Ti–O) values, (B) N(Ti(–O–)Ti) values, and (C) Fourier transform of k^3-weighted EXAFS χ function.

with the reversible change of the *N*(Ti–O) and *N*(Ti(–O–)Ti) values based on EXAFS analyses (Fig. 3A, B).

3.3. Photoconversion in CO_2 and moisture at 0.12–0.80 MPa

First, photoconversion tests at 0.40 MPa CO_2 and moisture are performed by changing the amount of Pd/TiO_2 photocatalyst between 100 mg and 10 mg. This is the most active photocatalyst among the catalysts in Eq. (3) under the reaction conditions from CO_2 and H_2 in reference 16; under CO_2 and moisture, it is methane-selective among C-containing compounds (>99–82 mol%; Table 3A-b, d). The total formation rate of C-containing products using 10 mg Pd/TiO_2 (23 μmol h^{-1} g_{cat}^{-1}) is higher by 16 times than that using 100 mg, probably due to the smaller reflectance/scattering by 10 mg of film. Thus, light absorption of 10 mg of film is more effective, in comparison to 100 mg powder. The peak due to low-energy anatase 1 0 1 plane is less intense by 26% for film in comparison to that in powder while high-energy anatase 1 0 3, 1 1 2, and ritile 1 0 1 planes are slightly favored relatively [16]. The energetically unstable 1 1 2 plane is preferred for a TiO_2 film formed via aerosol chemical vapor deposition of titanium iso-propoxide on to the substrate at 773 K, and it enhances its electron mobility [13]. The difference of preferred planes of film between this study (mean thickness 14 μm ± 3 μm, Fig. 1) and reference 13 (mean thickness 1.5 μm) would be due to the preparation procedure of film rather than the film thickness.

The total formation rates of C-containing compounds using moisture (Table 3B-i) are compared to the corresponding ones at the same total pressure using H_2 (Table 3B-ii) for Pd/TiO_2. Using Pd/TiO_2 at 0.40 MPa, the rate of 23 μmol-C h^{-1} g_{cat}^{-1} using moisture (Table 3A-d) is lower by 0.61 times than that using H_2 (Table 3B-d-i, ii) [16].

Based on the results of the photoconversion tests, we examine the mass balance under CO_2 and moisture using the following equations. *r* is the molar formation rate of the product.

$$r(O_2) = 2r(CH_4) + r(CO) + 1.5r(CH_3OH) + 0.5r(H_2)_{SR} \quad (14)$$

$$r(H_2) = r(CO) + r(H_2)_{SR} \quad (15)$$

The conversion of CO_2 into C-containing products via Eqs. (16)–(18) and a competing side reaction (SR) of water splitting (Eq. (19)) are considered. The reverse reaction of Eq. (19) is also taken into account to include the effect of a secondary reaction of formed H_2 with CO_2 to produce C-containing products and water [16].

$$CO_2(g) + 2H_2O(g) \rightarrow CH_4(g) + 2O_2(g) \quad (16)$$

$$CO_2(g) + H_2O(g) \rightarrow CO(g) + O_2(g) + H_2(g) \quad (17)$$

$$CO_2(g) + 2H_2O(g) \rightarrow CH_3OH(g) + 1.5O_2(g) \quad (18)$$

$$2H_2O(g) \Longleftrightarrow O_2(g) + 2H_2(g) \quad (19)$$

Based on Eq. (14), the theoretical O_2 amounts formed using Pd/TiO_2, in the tests at 0.40 MPa is 6.6 μmol in comparison to the detected O_2 amounts of 0.28 μmol (Tables 3A-d and 4d). Thus, only 4.2% O_2 is experimentally detected, suggesting that the formed O_2 is readsorbed and/or intermediate O species remain on the photocatalyst surface after the tests. The ratios of consumed holes versus consumed electrons is also listed in Table 4d, however, are not exactly the same as the ratios of experimentally detected O_2 versus theoretical one described above due to the contribution of side reaction in Eq. (14). Using Pd/TiO_2, O species are accumulated on TiO_2 after the photoconversion test, because some of the O sites are lost on/in TiO_2 during the photoconversion test but are restored after the test, as confirmed by the Ti K-edge XAFS analysis (Table 2B-c, e, e′ and Fig. 3).

Table 4
The balance of oxygen in the CO_2 Photoconversion tests (5 h) and FTIR monitoring (16 h) under various reaction conditions.

Entry	Photocatalysts		Reactants (MPa)		Theoretical O_2 formed for 5 h based on equation 14 (μmol)	Surface hydroxy group (μmol)	Surface hydroxy consumed (μmol) for 16 h	O_2 uptake for 1 + 5 h (μmol)	e^-'s consumed for total C-containing products for 5 h (μmol)	e^-'s consumed for H_2 for 5 h (μmol)	O_2 detected for 5 h (μmol; Table 3A)	Ratio of consumed h^+s/e^-'s based on product amounts
	Type	Wt (mg)	CO_2	H_2O								
a	Pd/TiO_2	100	0.003 4	0.001 2	2.6 (8.4 for 16 h)	7.0	24	0.75,[*1] 1.98 [*2]	0.90	6.9	0.13	0.060
d		10	0.40	0.002 3	6.6				8.0	18	0.28	0.043
d′[*3]					0.018				0.069	<0.002	<0.004	<0.058
d″[*4]					1.8				3.0	4.2	0.060	0.030
e[*5]			0.40[*5]	0[*5]	6.0				11	3.7	0.28	0.076
h	TiO_2		0.40	0.002 3	0.17				<0.06	0.67	<0.004	<0.024

[*1,*2]Measured under UV–visible light for 1 h^{-1} and under dark for 5 h.[*2]
[*3,*4]Using L42 filter[*3] and U330 filter[*4] at the light exit. Temperature = 296 K.
[*5]Mixed gas of 0.10 MPa of CO_2 and 2.3 kPa of H_2O was flowed prior to the introduction of 0.40 MPa of CO_2.

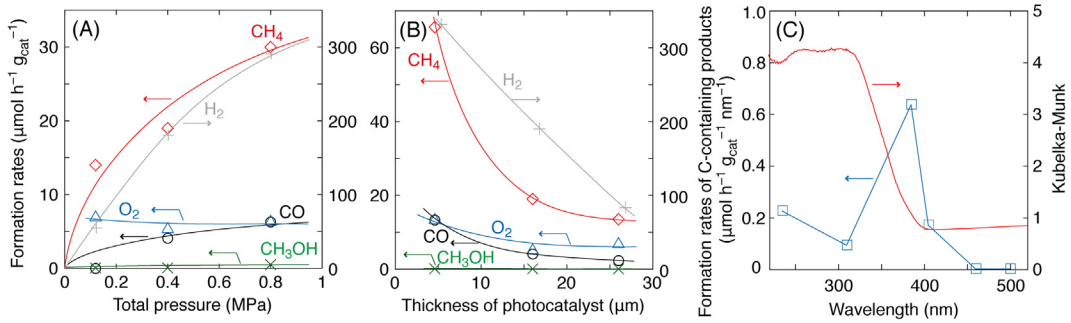

Fig. 4. (A) The dependence of formation rates for CH_4, CO, methanol, O_2, and H_2 on total reactant pressure and (B) on thickness of Pd/TiO_2 photocatalyst film both under the irradiation of UV–visible light from 500-W Xe arc lamp. (C) The dependence of total formation rates for C-containing products on the wavelength of irradiated light plotted with UV–visible absorption spectrum [16]. (A) Pd/TiO_2 10 mg, CO_2 0.12–0.80 MPa, and moisture 2.3 kPa. (B) Pd/TiO_2 4.6–26 μm-thick (namely 2.9–16 mg), CO_2 0.40 MPa, and moisture: 2.3 kPa. (C) Pd/TiO_2 10 mg, CO_2 0.40 MPa, and moisture 2.3 kPa.

The pressure dependence of the photoformation rates on CO_2 and moisture is investigated using Pd/TiO_2 (see also Supplementary material, Section S3). Major methane formation is preserved (Fig. 4A). At 0.12–0.80 MPa using 10 mg catalyst, the reaction order of methane, CO, and H_2 is 0.39, 0.62, and 0.89, respectively (Table 3A-c, d, and g and Fig. 4A). H_2 formation through Eq. (19) is accelerated by the increase of the CO_2 pressure [$P(CO_2)$], suggesting that it is correlated with the paths toward C-containing products via Eqs. (16)–(19). Using Pd/TiO_2 at 0.80 MPa, the total C-containing product formation rate using moisture was 37 μmol h^{-1} g_{cat}^{-1} (Table 3A-g and Fig. 4A) that was higher by 4.3 times than that using H_2 (Table 3B-g-i, ii).

The dependence of photoformation rates on Pd/TiO_2 film thickness was also investigated (Fig. 4B). On the basis of rates in the unit of μmol h^{-1} g_{cat}^{-1}, formation rates for methane and CO gradually increased as the mean thickness of Pd/TiO_2 decreased from 26 μm to 16 μm. In contrast, formation rates especially for methane dramatically boosted to 66 μmol-CH_4 h^{-1} g_{cat}^{-1} when the mean thickness further decreased from 16 μm to 4.6 μm, suggesting that upper layer of Pd/TiO_2 film was more effectively utilized for the photocatalysis as suggested in the color change of top 5 μm by cross-sectional SEM for sample after photocatalytic test (Fig. 1b2). H_2 photoproduction increased linearly as the catalyst thickness gradually decreased from 26 μm to 4.6 μm. The dependence for O_2 formation rates on film thickness was not clear (Fig. 4B).

As a control, 0.10 MPa CO_2 and 2.3 kPa moisture is input, and then photocatalytic testing is performed only in 0.40 MPa CO_2 (Table 3A-e). In comparison to the corresponding standard test under 0.40 MPa CO_2 and 2.3 kPa moisture (Table 3A-d), the C-containing product selectivity of 82 mol% for methane, 18 mol% for CO, and 0.21 mol% for methanol (Table 3A-e) remains essentially the same at 82, 18, and 0.27 mol%, respectively (Table 3A-d). However, the total formation rates of C-containing products increase by 1.32 times to 31 μmol-C h^{-1} g_{cat}^{-1} in the absence of moisture (Table 3A-e). This result suggests that water, which is stored as adsorbed or in the form of the hydroxy group during pretreatment, photoconverts CO_2 more efficiently. The theoretical O_2 amount formed is 6.0 μmol based on Eqs. (14) and (15) and accounts for only 4.6% of the experimental O_2 evolution (5.5 μmol h^{-1} g_{cat}^{-1} to 0.28 μmol, Tables 3A-e and 4e), similar to the theoretical/experimental ratio of 4.2% for standard testing under 0.40 MPa CO_2 and moisture (Table 3A-d). 30 μmol h^{-1} g_{cat}^{-1} water formation results due to the non-catalytic desorption of adsorbed water.

The hydroxy group population on TiO_2 is 7 nm^{-2} based on the specific surface area, the dependence of stretching vibration peak intensity of hydroxy (ν_{OH}) in FTIR on calcination temperature, desorbed water amount based on GC as a function of calcination temperature, and/or the monitoring of the ratio of ν_{OD}/ν_{OH} in the presence of D_2 gas [45], corresponding to $0.010 \times 60 \times 10^{18} \times 7/(6.02 \times 10^{23}) = 7.0$ μmol in the 10 mg Pd/TiO_2 photocatalyst used for the kinetic tests under CO_2 only (Tables 3A-e and 4e). The formation rates of the C-containing products and H_2 (31 and 37 μmol h^{-1} g_{cat}^{-1}) correspond to 11 and 3.7 μmol-e^- reduction, respectively (Tables 3A-e and 4e). The oxidation reaction of the 7.0 μmol of surface hydroxy groups by photogenerated h^+'s via Eqs. (4′) and (5) (14 μmol-e^- oxidation) accounts for 98% of the reduction to the C-containing products and H_2 (total 15 μmol-e^-; Table 4e). surface O species and/or adsorbed water are expected to participate in the oxidation via Eqs. (5′) and (4), respectively, as implied by the increase of the O_V sites in/on TiO_2 based on Ti K-edge EXAFS (Table 2B-e′ and Fig. 3). The absence of moisture during irradiation testing would alleviate the blocking of the O_V sites for the activation of CO_2-derived species.

The other control tests are performed by controlling four factors (see the *Experimental*) in order to compare the results with those of the test at 0.40 MPa using 10 mg Pd/TiO_2 (Table 3A-d). In the absence of reactants or in the absence of a catalyst (Table 3A-d′′′′, i), no C-containing products, H_2, nor O_2 are detected after 5 h of UV–visible light irradiation. Water formation at the rate of 8.2 μmol h^{-1} g_{cat}^{-1} in the absence of reactants results merely due to desorption from the catalyst. Using TiO_2, no C-containing products are detected, but H_2 is formed at a 3.7% rate of that using Pd/TiO_2 (Table 3A-d, h), demonstrating that Pd is indispensable for converting CO_2 using moisture. O_V sites are artificially created in vacuum irradiated under UV–visible light (Fig. 5b). However, no C-containing products are detected and H_2 formation rate remains low under the reaction conditions (Table 3A-h′), demonstrating that the rate of Eq. (2) on Pd is by far higher than those of Eqs. (6)–(8) on the O_V sites [5–8,23,24]. The theoretical O_2 amount formed is 0.17 μmol versus an experimental O_2 evolution less than the detection limit of GC–TCD (<0.004 μmol), reconfirming that the O_2 and/or O species are readsorbed/remain on TiO_2.

A control test in the absence of CO_2 produces no C-containing products (Table 3A-f), demonstrating that the C source in the photoconversion tests is exclusively CO_2 in this study. This result is consistent with $^{13}CH_4$ formation using $^{13}CO_2$ and moisture monitored by FTIR (Fig. 7C-b). H_2 is effectively formed at the rate of 106 μmol h^{-1} g_{cat}^{-1} in the presence of moisture only. The rate decreases by 0.59 times compared to that under 0.40 MPa CO_2 and moisture (Table 3A-d, f), demonstrating that reduction reaction paths to C-containing products and H_2 (Eqs. (16)–(19)) are correlated.

Furthermore, we perform a control test by filtering out UV light of λ < 420 nm. In this case, no methane, CO, nor H_2 is formed above

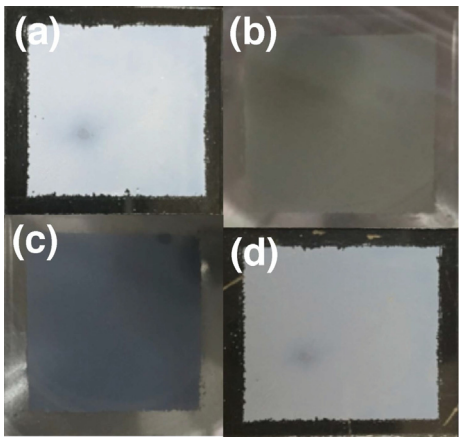

Fig. 5. The color changes of TiO_2 (P25) film as fresh (a), under vacuum and UV–visible light for 4 h (b), under 0.40 MPa CO_2 and moisture for 3 h (c), and after the test and exposed to air (d).

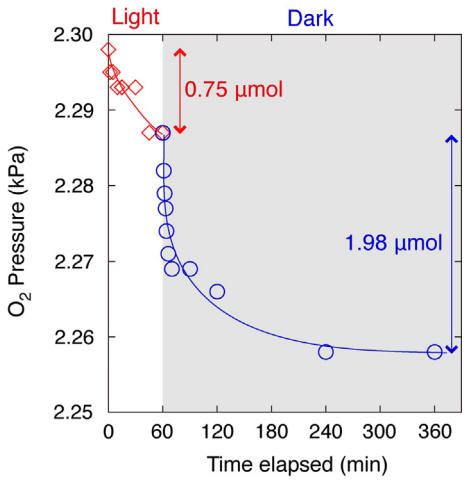

Fig. 6. Monitoring of O_2 uptake (2.3 kPa at 0 min) on Pd/TiO_2 photocatalyst after UV–visible light irradiation in vacuum for 5 h. Under UV–visible light for 1 h followed by 5 h under dark.

the detection limit (Table 3A-d′). A small amount of methanol is detected, but the total formation rate of C-containing compounds is only 1.0% of that irradiated under UV–visible light (Table 3A-d). The theoretical O_2 amount formed is 0.018 μmol versus no O_2 evolution above the detection limit (<0.004 μmol; Table 4d′). In the other blank test conducted by removing UV light with $\lambda < 250$ nm and most of the visible light ($390 < \lambda < 695$ nm), methane is formed predominantly, but the rate is lower by 0.39 times in comparison to that under UV–visible light (Table 3A-d″, d). The theoretical O_2 amount formed is 1.8 μmol against an experimental O_2 evolution of 0.060 μmol (Table 4d″). Only 3.3% of the stoichiometric O_2 is detected, similar to 4.2% in the test under full light. The H_2 evolution rate is lower by 0.23 times compared to that in the test under full light. Thus, in both control tests, O_2 adsorbs again after irradiation, and the visible light contributes to producing C-containing products as well as H_2 via SPR [16] on Pd.

In the absence of UV–visible light at 299 K (Table 3A-d‴, d), no C-containing products, H_2, nor O_2 are detected. The photoreduction of CO_2 using moisture and water photosplitting via Eqs. (16)–(19) are endothermal, in contrast that the photoreduction of CO_2 into methane using H_2 that is exothermal [16]. In this context, to verify the thermal effects, blank tests in the absence of UV–visible light are also carried out at 353 K (Table 3A-d⁗). No products are detected above the detection limit, demonstrating that the CO_2 conversion from CO_2 and moisture shown in Table 3A proceeds entirely photocatalytically.

3.4. O_2 uptake measurements in the presence/absence of UV–visible light

The O_2 formation in typical reaction conditions (0.40 MPa CO_2 and moisture, 10 mg photocatalyst) was only 4.2% compared to the stoichiometry of Eqs. (14) and (15) to form methane, CO, methanol, and H_2 (Tables 3A-d and 4d). The Pd/TiO_2 photocatalyst was previously irradiated under UV–visible light in vacuum for 5 h. O_2 pressure decreased starting from 2.298 kPa to 2.287 kPa (Fig. 6, left), corresponding to 0.75 μmol of O_2 uptake (Table 4a).

Next, the monitoring of O_2 pressure was continued under dark conditions (Fig. 6, right). The pressure quickly decreased in the first 30 min by more than 0.02 kPa and converged to 2.258 kPa after 5 h. Therefore, 1.98 μmol of O_2 adsorbed on Pd/TiO_2 under dark (Table 4a). The theoretical O_2 amount formed using 100 mg Pd/TiO_2 in the photoconversion test at 4.6 kPa for 5 h was 2.6 μmol based on Eqs. (14) and (15) and the rate in Table 3A-a, versus the experimental formation of 0.13 μmol based on Eqs. (14) and (15) and Table 3A-a (Table 4a). The difference (2.5 μmol) can be rationalized by the adsorption on TiO_2, 0.75 + 1.98 = 2.73 μmol (Fig. 6 and Table 4a).

The difference between the theoretical O_2 amount formed (6.6 μmol) and the O_2 amount detected (0.28 μmol) in the CO_2 photoconversion test at 0.40 MPa using 10 mg Pd/TiO_2 (Table 4d) was greater (6.3 μmol) than that at 4.6 kPa using 100 mg of Pd/TiO_2 (Table 4a), mostly due to the difference in the reaction pressure and the thickness of the photocatalyst.

The oxygen balance was summarized in Table 4. Stoichiometric O_2 following Eqs. (16)–(19) was not detected for all the catalysts, however, the unbalance would be consistently explained by the participation of surface hydroxy groups via Eqs. (4′) and (5) and/or readsorption of O_2 after photocatalytic tests (Fig. 6).

Thus, the evidences of O_V sites were the decrease of N(Ti–O) values based on Ti K-edge EXAFS (Table 2B and Fig. S2B), the decrease and increase of both N(Ti–O) and N(Ti(–O–)Ti) values during the irradiation of UV–visible light and under dark, respectively (Fig. 3A, B), color change at surface 5 μm layer in cross-sectional SEM (Fig. 1b2), color change of photocatalyst (Fig. 5b, c), and the O_2 adsorption tests under UV–visible irradiation and under dark (Fig. 6). These evidences strongly suggest the occurrence of Eq. (1) via Eqs. (4) and (5) and/or Eqs. (4) and (5′), however, the partial O_2 readsorption even under light (Fig. 6) means that the turnover of Eq. (1) was not completed and an O_2-removing reagent would be needed to proceed true catalysis following Eq. (1).

3.5. FTIR during the photoconversion in CO_2 and moisture

The intermediate species during the efficient conversion of CO_2 into major methane and H_2 on Pd/TiO_2 is monitored using FTIR. In the spectrum for fresh Pd/TiO_2 in vacuum at 293 K for 2 h, two sharp peaks at 3673 and 3634 cm^{-1}, a very broad peak between 3500 and 3000 cm^{-1}, a sharp peak at 1624 cm^{-1}, and weaker peaks at 1553, 1438, and 1358 cm^{-1} are observed (Fig. 7A-a). These peaks can be assigned to ν_{OH} of H-bound hydroxy, bi or tricoordinated hydroxy, and H-bound water [46], antisymmetric stretching vibration (ν_{as}) of hydrogencarbonate (HO–CO_2Ti), ν_{as} of bidentate carbonate (O–CO_2Ti), symmetric stretching vibration (ν_s) of hydrogencarbonate, and ν_s of bidentate carbonate [47], respectively.

When 3.4 kPa CO_2 and 1.2 kPa moisture are introduced into the photocatalyst (Fig. 7A-b), the peak intensity for both pairs of hydrogen carbonate and bidentate carbonate increase, while a part of the two hydroxy peaks at 3673 and 3634 cm^{-1} switches to a

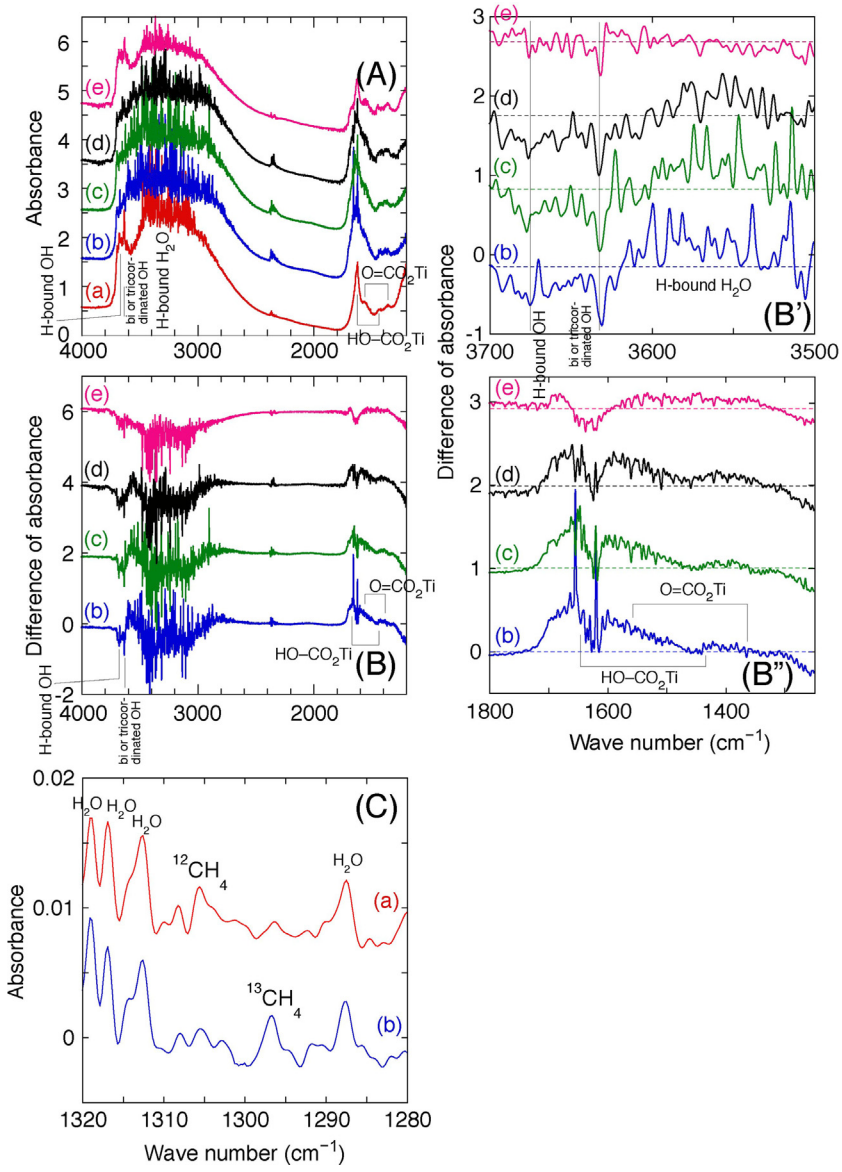

Fig. 7. (A) FTIR spectra for Pd/TiO_2 photocatalyst in vacuum for 2 h (a), CO_2 (3.4 kPa) and moisture (1.2 kPa) added (b), under irradiation of UV–visible light for 15 min (c) and for 16 h (d), and light is turned off after 16 h of the reaction and evacuated for 20 min (e). (B) Difference spectra: A-b–A-a – the spectrum of CO_2 (3.4 kPa) – the spectrum of moisture (1.2 kPa) (b), A-c–A-a – the spectrum of CO_2 (3.4 kPa) – the spectrum of moisture (1.2 kPa) (c), A-d–A-a – the spectrum of CO_2 (3.4 kPa) – the spectrum of moisture (1.2 kPa) (d), and A-e – A-a (e). (B′), (B″) Expanded views of B in the regions of stretching vibrations of O–H (B′) and O–C–O (B″). (C) FTIR monitoring of reactants and products using Pd/TiO_2, UV–visible light, CO_2 (59 kPa), and moisture (2.3 kPa). Natural CO_2 for (a) versus $^{13}CO_2$ (^{13}C 99%) for (b).

broad peak due to H-bound water (~3550 cm^{-1}). These changes are more evident if spectrum A-b is subtracted from spectrum A-a, and further subtracted from the spectra of CO_2 (3.4 kPa) and moisture (1.2 kPa) (Fig. 7B-b and 7B′-b; decrease of two OH peaks versus increase of broad water peak).

Then, the Pd/TiO_2 sample under CO_2 and moisture is irradiated with UV–visible light for 15 min (Fig. 7A-c) and 16 h (Fig. 7A-d). The extent of the change can be checked when the spectra under light is subtracted from spectrum A-a and further subtracted from the spectra of CO_2 (3.4 kPa) and moisture (1.2 kPa) (Fig. 7B-c, d). The expanded views are shown for O–H region (Fig. 7B′-c, d) and O–C–O region (B″-c, d). The hydrogen carbonate and bidentate carbonate species are inert, and the peaks due to these species negligibly change starting from spectrum b to c then d (Fig. 7B″), whereas peaks due to H-bound and di/tri-coordinated hydroxy groups decrease in Fig. 7B-d compared to Fig. 7B-b and c via the reactions of Eqs. (4′) and (5).

Finally, the UV–visible light is turned off, and the Pd/TiO_2 photocatalyst is evacuated at 293 K for 20 min (Fig. 7A-e). The change is more evident, if the difference between spectra B-e and B-d is compared in order to extract the change of the surface species compared to the original spectrum a (Fig. 7B-e). The expanded views are also shown in Fig. 7B′-e and B″-e. The decrease of both the H-bound and the bi/tri-coordinated hydroxy group during the photoconversion test is canceled via the reaction

$$H_2O(g) + O_V + O(\text{surface}) \rightarrow 2OH(\text{surface}) \quad (20)$$

The amount of hydrogen carbonate and bidentate carbonate species decreases to the level before the photoconversion test by the evacuation of ambient CO_2 (Fig. 7B″-e). We assume that the surface concentration of hydroxy is 7 nm^{-2} for Pd/TiO_2 evacuated at 290 K (Fig. 7A-a) [45], and the peak area of total ν_{OH} in Fig. 7A-a decreases by 0.66 times after the 16 h of the CO_2 photoconversion test (Fig. 7A-d). Thus, $0.10 \times 60 \times 10^{18} \times 7 \times 0.34/$

(6.02×10^{23}) = 24 μmol of the hydroxy group on 100 mg of the Pd/TiO_2 disk are consumed during the FTIR measurements under 4.6 kPa CO_2 and moisture and UV–visible light for 16 h (Table 4a). Thus, 24 and 12 μmol O_2 are formed via Eqs. (4) and (5) and Eqs. (4′) and (5), respectively. The O_2 amount assuming the route of Eqs. (4′) and (5) agrees more with the theoretical (stoichiometric) O_2 formation (5.3 μmol h^{-1} $g_{cat}^{-1} \times 0.100 \times 16$ = 8.4 μmol; Table 4a) in the photoconversion test at 4.6 kPa CO_2 and moisture based on the total formation of methane and H_2 (Table 3A-a) and Eqs. (14) and (15). The observed O_2 formation (0.25 μmol h^{-1} g_{cat}^{-1} corresponding to 0.40 μmol-O_2) suggests readsorption of O_2 on the TiO_2 surface. In summary, the intensity of the hydrogen carbonate and bidentate carbonate peaks on the TiO_2 surface partially increases in the presence of CO_2 and moisture, but changes slightly due to UV–visible irradiation. The peak intensity due to the H-bound and the di/tri-coordinated hydroxy group for fresh Pd/TiO_2 decreases by 0.66 times after the 16 h of CO_2 photoconversion, demonstrating that the reactions of Eqs. (4′) and (5) for O_2 formation proceed.

The reactants and products were also monitored using CO_2 (59 kPa), moisture (2.3 kPa), Pd/TiO_2 photocatalyst, and UV–visible light. When natural CO_2 (^{12}C 98.93%, ^{13}C 1.07%) and moisture was employed, a peak at 1306 cm^{-1} appeared that was assigned to bending vibration mode (ν_4) of $^{12}CH_4$ whereas a peak at 1297 cm^{-1} appeared that was assigned to ν_4 of $^{13}CH_4$ using $^{13}CO_2$ and moisture (Fig. 7C). The isotope shift was in consistent with values in literature [48–50] taking the low concentrations of methane due to kinetic tests using low pressure of $^{13}CO_2$ (59 kPa) into account. This result was in accordance with the blank test under moisture (2.3 kPa) and UV–visible light in which no C-containing products were detected (Table 3A-f).

4. Discussion

4.1. Electronic excitation of Pd/TiO_2 photocatalyst

The performance of photocatalysts is compared at nearly optimized conditions: using 10 mg photocatalyst film under 0.40 MPa CO_2 and moisture (Table 3A-d). The photocatalytic activity to form total C-containing compounds from CO_2 and H_2 was not correlated to the E_g values of the metal oxide (3.1–3.2 eV for Pd/TiO_2) or the conduction band (CB) minimum voltage for the semiconductors (−0.1 at pH 0, Scheme 1A) [16]. The work functions (WFs) for Pd are 5.22–5.6 eV versus the vacuum level [34], corresponding to potentials of 0.78–1.16 V versus SHE (pH 0), which are slightly positive compared to the CB of TiO_2 (−0.1 V). Namely, the potential for achieving electron trapping levels are a little more positive than the reduction potentials of methane (0.17 V @pH 0) or CO (0.30 or −0.12 V @pH 0) (Scheme 1A) [9,51], and it is difficult to reduce CO_2.

In UV–visible absorption spectra [16], the absorption extended over the range between 400 and 800 nm of visible light for Pd/TiO_2. [Localized] SPR is a collective vibration of electrons near surface in the resonant condition that natural frequency of the electrons forced by the positive charge of nucleus coincides with the frequency of light. SPR results in elevated electric fields at the surface of the Pd nanoparticles (Scheme 1A). The elevated fields yield a greater number of electron–hole pairs [18,52]. It is also known that the resonance frequency of SPR increases as the metal nanoparticles size decrease [52]. In HR-TEM images for Pd/TiO_2 photocatalyst, 1.0–6.5 nm of Pd nanoparticles were observed on TiO_2 surface [16]. Hence, hot electrons due to SPR at Pd nanoparticles, especially relatively smaller ones, would gain sufficient energy relative to the reaction potential of CO_2/CH_4 and transfer to CO_2-derived surface species (Scheme 1A).

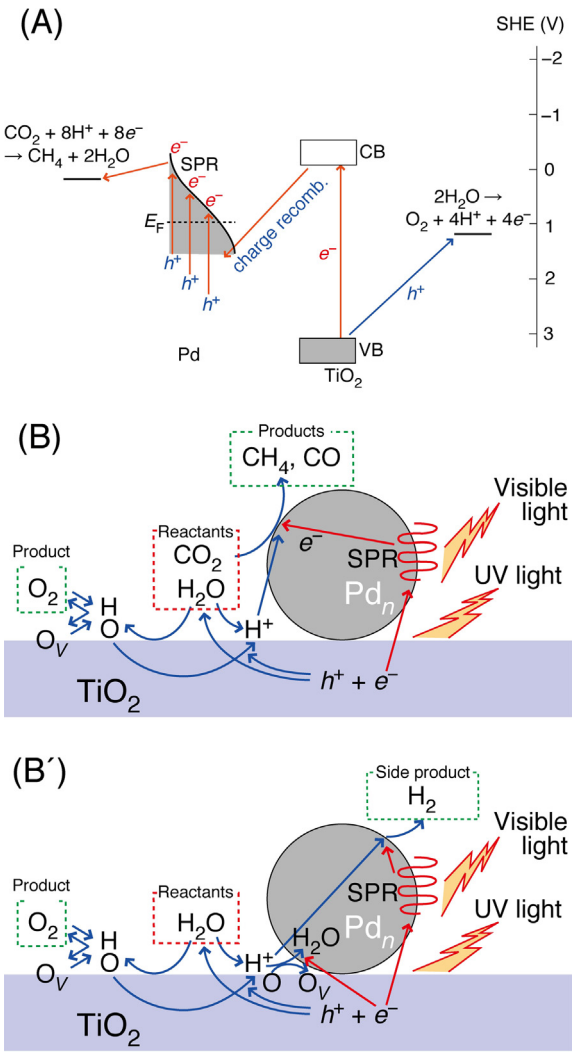

Scheme 1. (A) Energetic diagram of CO_2 photoconversion using moisture (pH 0), (B) proposed reaction mechanism of CO_2 photoconversion using moisture, and (B′) that of side reaction to form H_2.

If the positive charge that remains at the Pd nanoparticles is combined with excited electrons trapped from the CB of TiO_2, the *Z-scheme*-like redox combination is completed. In this context, the electron trapping at metal nanoparticles excited from the semiconductors must be followed by the transfer of hot/excited electrons produced due to SPR on metal nanoparticles to CO_2-derived species [16,21]. This proposed electron flow diagram (Scheme 1A) is well in accord with the wavelength dependence of irradiation for Pd/TiO_2 (Table 3A-d, d′, d″). The sum of C-containing product formation rates under visible light (0.23 μmol h^{-1} g_{cat}^{-1}) and under UV light (7.4 μmol h^{-1} g_{cat}^{-1}) does not account for the rate under UV–visible light (23 μmol h^{-1} g_{cat}^{-1}), demonstrating a synergistic effect, e.g., by UV for the BG excitation of TiO_2 and by visible light for the hot electron by SPR.

As the d-band positions at 2.4–4 eV below the Fermi energy (E_F) level [18], the hot electrons in Pd/TiO_2 catalyst would be mostly due to intraband excitation within conduction band (∼visible light region) [18,52] of 1.0–6.5 nm of Pd nanoparticles rather than due to interband transition between d-band and conduction band (∼UV light region) [18,53].

Similar photoconversion rates in CO_2 and moisture into methane and CO are reported by the addition of metal to TiO_2 in the same order, Pt > Pd > Au > Rh > Ag, as that of WF [6]. Very small

metal nanoparticles are preferred, because the E_F level rises, but still remains below the CB minimum due to the quantum confinement for CO_2 reduction [13]. The effects of quantum confinement should be minimal for Pd particles with a mean size of 1.1–3.1 nm (Table 1) in this study.

4.2. Cause of higher reactivity of moisture than H_2 in CO_2 photoconversion at 0.80 MPa

At 0.40 MPa, the total photoformation rates of C-containing products in CO_2 and moisture are lower by 0.61 times than those in CO_2 and H_2 using Pd/TiO_2 (Table 3B-d). Furthermore, using Pd/TiO_2 at 0.80 MPa, the total C-containing product formation rate using moisture becomes higher by 4.3 times than that using H_2 (Table 3B-g). Thus, at the optimized reaction pressure, moisture is more reactive than H_2 for pressurized CO_2 photoconversion. In our preliminary photocatalytic tests under 0.40 MPa of CO_2 and moisture using several semiconductor-based photocatalysts, i.e. similar conditions to those in Table 3A-d, the total C-containing product formation rates were higher than those in tests under corresponding reactant pressure of CO_2 and H_2 (Supplementary material, Section S4 and Table S2) [16]. The experimental O_2 formation was 40–3.2% of corresponding theoretical values based on Eqs. (14) and (15) (Table S3) in comparison to 4.2% for Pd/TiO_2 (Table 3). In contrast, quite fast photo-assisted methane formation was reported under CO_2, H_2, visible light ($\lambda > 450$ nm), and Ni/SiO_2·Al_2O_3. Thermal effect nearly at 423 K was suggested due to heat of reaction for methane formation from CO_2 and H_2 [54]. In this context, the comparison of reactivity between moisture and H_2 depends on reaction temperature. No thermal effects were found using Pd/TiO_2 at 299–353 K in this study (Table 3A-d‴, d⁗). The contribution of the secondary reaction of CO_2 with formed H_2 from moisture is negligible (Supplementary material, Section S6).

Following, we consider the oxidation reaction using moisture or H_2 on semiconductors combined with Pd nanoparticles. Water is activated by a hole to form the **·**OH radical (Eq. (4)) [7]. The subsequent reaction of **·**OH with a surface hydroxy group/O atom is fast [41], e.g., to form O_2, an O_V site, and a proton(s) (Eqs. (5) or (5′) and Scheme 1B, left) due to the nature of the radical reaction. In fact, the concentration of O_V sites dramatically increases on/in TiO_2 as monitored by the decrease of the N(Ti–O) value from 5.4 for fresh sample to as low as 3.5 under UV–visible light irradiation at beamline (Table 2B-c, e′ and Fig. S2B-c, e′). This change was supported by the monitoring of N(Ti–O) and N(Ti(–O–)Ti) values during the irradiation of UV–visible light (3.5 h) and darkness (0.5 h) (Fig. 3). The protons formed near the interface between the metal nanoparticle and the TiO_2 surface (Eq. (4)) are transferred to the metal nanoparticle to form C-containing products or H_2, whether they encounter CO_2-derived species and hot/excited electrons, or such electrons only (Scheme 1B, right). In clear contrast, O_V sites are observed only at the interface between Pd and the TiO_2 surface under CO_2 and H_2 and UV–visible light [16], denying the radical oxidation mechanism from H_2. Effectively separated redox sites are nicely conjugated to transport protons between them (Scheme 1B), similar to photosystems [4].

In contrast, both CO_2 reduction and H_2 oxidation may proceed on Pd using Pd/TiO_2 [16]. Due to the competitive adsorption of CO_2 and H on Pd, the exclusive methane formation rates produce a volcano-like maximum at $P(CO_2)$ of 0.12 MPa and at $P(H_2)$ of 0.28 MPa in the contour diagram. Thus, effective redox-site separation between TiO_2 surface for H_2O oxidation and Pd nanoparticles for CO_2 reduction is the reason of the observed higher reactivity of moisture than H_2 using Pd/TiO_2. Redox-site separation is also deduced from the reaction order of methane and CO formation on $P(CO_2)$ (0.39 and 0.62, respectively; Fig. 4A), in clear contrast to the volcano-like pressure dependence peaking at $P(H_2)$ = 0.28 MPa and $P(CO_2)$ = 0.12 MPa using CO_2 and H_2 [16].

The best CO_2 photoformation rate of C-containing compounds in this study is 37 μmol h^{-1} g_{cat}^{-1} using Pd/TiO_2. The photo in-profile (action) spectrum for Pd/TiO_2 photocatalyst peaked at 385 nm, but the action also increased in the UV light region based on the tests using seven kinds of cut filters (Fig. 4C), suggesting the needs of both UV light for BG excitation for TiO_2 and UV/visible light for SPR for Pd nanoparticles for the photoconversion (Scheme 1A). Please note that the peak centered at 385 nm was drawn based on tests under the conditions of the presence of UV light of $\lambda < 370$ nm. Thus, if we simplify the quantum efficiency as the ratio of total electrons needed to form C-containing products from CO_2 in the photo in-profile spectrum between 358 nm and 412 nm (7.6×10^{-4} μmol-e^- s^{-1}) versus the photon number of absorbed/scattered/reflected UV–visible light between 358 nm and 412 nm (2.9×10^{15} photons $s^{-1} \times 0.49$) based on the data that 51% of incident UV–visible light transmits the film (see Section 2.3), quantum efficiency for Table 3A-g was 16%. This is the upper limit of true quantum efficiency because the proposed mechanism in Scheme 1A requiring light for both BG excitation and SPR cannot be plotted in simple two-dimensional action spectrum as in Fig. 4C. In the evaluation above, the photon number of UV light is not included.

The best rate in this study is lower compared to 1400–2200 μmol-CH_4 h^{-1} g_{cat}^{-1} using Pt-TiO_2 (mean thickness ~ 1.5 μm) [13] or Au-Cu-TiO_2 films (0.48 mg cm^{-2}) [5]. In the cross-sectional SEM image, 5 μm of TiO_2 layer including more O_V sites are detected at the upper part of the 15 μm ± 3 μm-thick Pd-TiO_2 layer (Fig. 1b2). The upper 5 μm of the TiO_2 layer absorbs more photons to proceed reactions 4, 4′, 5, and/or 5′. In fact, the rate of major methane formation dramatically boosted when the mean thickness of Pd/TiO_2 film decreased from 16 μm to 4.6 μm (Fig. 4B). Thus, even a thinner catalyst film is needed to improve the photoconversion rate of CO_2 in this study.

Liu et al. suggested that CO_2 activation on an O_V site forms CO via Eqs. (6) and/or (7) + (8) [7]. O_V sites should be distributed in the upper 5 μm of the TiO_2 layer (Fig. 1b2) during UV–visible light exposure under 0.40 MPa CO_2 and moisture (Fig. 1b2 and Table 2A-e, B-e′). In contrast, O_V sites are detected only at the interface between Pd nanoparticles and the TiO_2 surface for Pd/TiO_2 under 0.40 MPa CO_2 and H_2 [16]. Based on the test using artificially created O_V sites on TiO_2 (Table 3A-h′ and Fig. 5b), direct CO_2 activation on O_V sites is negligible in comparison to that over Pd or the other reduction sites in this study.

Stoichiometric O_2 formation is not detected during CO_2 photoconversion according to Eqs. (14) and (15), but only 4.2% O_2 is experimentally detected for Pd/TiO_2 (Table 3A). The possibility of H_2O_2 formation is investigated using Ti sulfate, but it is not detected above the detection limit of 0.20 μmol (Supplementary material, Section S5) in comparison to the theoretical (stoichiometric) O_2 amount formed: 6.6 μmol using Pd/TiO_2 at 0.40 MPa (Tables 3A-d and 4d). Thus, the possibility of H_2O_2 formation is low, but, instead, the formed O_2 may be readsorbed by the photocatalysts after the photoconversion test but before the GC–TCD analysis, as shown in Fig. 6.

5. Conclusions

Photoconversion of CO_2 was optimized using moisture at 4.6 kPa–0.80 MPa. The result was successfully explained based on the levels of hot electrons due to SPR or BG-excited electrons.

At 0.80 MPa, moisture was found to be more reactive than H_2 for CO_2 photoconversion. This finding was attributed to the effective site separation between CO_2 reduction on Pd nanoparticles

and water oxidation on the semiconductor surface, as confirmed using in situ monitoring of Ti K-edge EXAFS and cross-sectional SEM. The redox sites were conjugated in order to transport protons effectively, in a way similar to photosystems. The mass balance of O is explained by the readsorption of the formed O_2 after the photoconversion test, because O_2 adsorption on the O_V sites was quicker under dark rather than under UV–visible light. CO_2 photoconversion rates increased up to 0.80 MPa CO_2 and moisture in a reaction order of 0.39–0.62 using Pd/TiO_2, whereas the volcano-like maxima were at $P(CO_2)$ of 0.12 MPa and $P(H_2)$ of 0.28 MPa in the contour plot.

Acknowledgements

The authors are grateful for the financial supports from the Grant-in-Aid for Scientific Research C (26410204) from Japan Society for the Promotion of Science and Leading Research Promotion Program (2015–) from the Institute for Global Prominent Research, Chiba University. X-ray absorption experiments were conducted under the approval of the Photon Factory Proposal Review Committee (2016G577, 2015G586, 2014G631). The authors thank Masaya Miyano for the support of data analysis. In addition, the authors would like to thank Enago (www.enago.jp) for the English language review.

Appendix A. Supplementary material

Supplementary data associated with this article can be found, in the online version, at http://dx.doi.org/10.1016/j.jcat.2017.06.016.

References

[1] Y. Izumi, Advances in CO_2 capture, sequestration, and conversion, in: F. Jin, L.-N. He, Y.H. Hu (Eds.), ACS Books, vol. 1194, Washingston, DC, 2015, pp. 1–46.
[2] Y. Izumi, Coord. Chem. Rev. 257 (2013) 171–186.
[3] S.N. Habisreutinger, L. Schmidt-Mende, J.K. Stolarczyk, Angew. Chem. Int. Ed. 52 (2013) 7372–7408.
[4] D. Voet, J.G. Voet, Biochemistry, second ed., J. Wiley & Sons, New York, 1995, p. 639.
[5] Ş. Neaţu, J.A. Maciá-Agulló, P. Concepción, H. Garcia, J. Am. Chem. Soc. 136 (2014) 15969–15976.
[6] S. Xie, Y. Wang, Q. Zhang, W. Deng, Y. Wang, ACS Catal. 4 (2014) 3644–3653.
[7] L. Liu, H. Zhao, J.M. Andino, Y. Li, ACS Catal. 2 (2012) 1817–1828.
[8] L. Liu, Y. Jiang, H. Zhao, J. Chen, J. Cheng, K. Yang, Y. Li, ACS Catal. 6 (2016) 1097–1108.
[9] F. Galli, M. Compagnoni, D. Vitali, C. Pirola, C.L. Bianchi, A. Villa, L. Prati, I. Rosetti, Appl. Catal. B 200 (2017) 386–391.
[10] I. Rossetti, A. Villa, M. Compagnoni, L. Prati, G. Ramis, C. Pirola, C.L. Bianchi, W. Wang, D. Wang, Catal. Sci. Technol. 5 (2015) 4481–4487.
[11] I. Rossetti, A. Villa, C. Pirola, L. Prati, G. Ramis, RSC Adv. 4 (2014) 28883–28885.
[12] R. Li, J. Hu, M. Deng, H. Wang, X. Wang, Y. Hu, H.-L. Jiang, J. Jiang, Q. Zhang, Y. Xie, Y. Xiong, Adv. Mater. 26 (2014) 4783–4788.
[13] W.N. Wang, W.J. An, B. Ramalingam, S. Mukherjee, D.M. Niedzwiedzki, S. Gangopadhyay, P. Biswas, J. Am. Chem. Soc. 134 (2012) 11276–11281.
[14] C.C. Yang, Y.H. Yu, B. van der Linden, J.C.S. Wu, G. Mul, J. Am. Chem. Soc. 132 (2010) 8398–8406.
[15] T. Yui, A. Kan, C. Saitoh, K. Koide, T. Ibusuki, O. Ishitani, ACS Appl. Mater. Interf. 3 (2011) 2594–2600.
[16] S. Kawamura, H. Zhang, M. Tamba, T. Kojima, M. Miyano, Y. Yoshida, M. Yoshiba, Y. Izumi, J. Catal. 345 (2017) 39–52.
[17] M. Miyano, H. Zhang, M. Yoshiba, Y. Izumi, Energy Technol. 5 (2017) 892–900.
[18] C. Clavero, Nat. Photon. 8 (2014) 95–103.
[19] N. Ahmed, Y. Shibata, T. Taniguchi, Y. Izumi, J. Catal. 279 (2011) 123–135.
[20] N. Ahmed, M. Morikawa, Y. Izumi, Catal. Today 185 (2012) 263–269.
[21] S. Kawamura, M.C. Puscasu, Y. Yoshida, Y. Izumi, G. Carja, Appl. Catal. A 504 (2015) 238–247.
[22] M. Morikawa, Y. Ogura, N. Ahmed, S. Kawamura, G. Mikami, S. Okamoto, Y. Izumi, Catal Sci. Technol. 4 (2014) 1644–1651.
[23] Y. Ji, Y. Luo, J. Am. Chem. Soc. 138 (2016) 15896–15902.
[24] D. Lee, Y. Kanai, J. Am. Chem. Soc. 134 (2012) 20266–20269.
[25] Y. He, Y. Wang, L. Zhang, B. Teng, M. Fan, Appl. Catal. B 168 (2015) 1–8.
[26] M.A. Asi, L. Zhu, C. He, V.K. Sharma, D. Shu, S. Li, J. Yang, Y. Xiong, Catal. Today 216 (2013) 268–275.
[27] J.A. Bearden, Rev. Mod. Phys. 39 (1967) 78–124.
[28] Y. Fujishima, S. Okamoto, M. Yoshiba, T. Itoi, S. Kawamura, Y. Yoshida, Y. Ogura, Y. Izumi, J. Mater. Chem. A 3 (2015) 8389–8404.
[29] Y. Ogura, S. Okamoto, T. Itoi, Y. Fujishima, Y. Yoshida, Y. Izumi, Chem. Commun. 50 (2014) 3067–3070.
[30] F.W. Lytle, R.B. Greegor, D.R. Sandstrom, E.C. Marques, J. Wong, C.L. Spiro, G.P. Huffman, F.E. Huggins, Nucl. Instrum. Methods Phys. Res. 226 (1984) 542–548.
[31] Y. Izumi, T. Itoi, S. Peng, K. Oka, Y. Shibata, J. Phys. Chem. C 113 (2009) 6706–6718.
[32] M. Morikawa, N. Ahmed, Y. Yoshida, Y. Izumi, Appl. Catal. B 144 (2014) 561–569.
[33] M. Vaarkamp, H. Linders, D. Koningsberger, XDAP Version 2.2.7, XAFS Services International, Woudenberg, The Netherlands, 2006.
[34] W.M. Haynes, D.R. Lide, T.J. Bruno, CRC Handbook of Chemistry and Physics, 96th Ed., CRC Press, Boca Raton, USA, 2015, Sections 12–17 and 12–122.
[35] A.G. Christy, S.M. Clark, Phys. Rev. B 52 (1995) 9259–9265.
[36] B.G. Hyde, S. Andersson, Inorganic Crystal Structures, John Wiley & Sons, New York, 1989, p. 67.
[37] D.T. Cromer, K. Herrington, J. Am. Chem. Soc. 77 (1955) 4708–4709.
[38] http://www.tokina.co.jp/io-filters/filters/sharp-cut-filters.html.
[39] http://www.tokina.co.jp/io-filters/filters/ut-va-filter.html.
[40] B.J. Kip, F.B.M. Duivenvoorden, D.C. Koningsberger, R. Prins, J. Catal. 105 (1987) 26–38.
[41] M.R. Hoffmann, S.T. Martin, W. Choi, D.W. Bahnemann, Chem. Rev. 95 (1995) 69–96.
[42] H. Yoshitake, T. Sugihara, T. Tatsumi, Phys. Chem. Chem. Phys. 5 (2003) 767–772.
[43] F. Farges, G.E. Brown Jr., J.J. Rehr, Phys. Rev. B 56 (1997) 1809–1819.
[44] F. Farges, G.E. Brown Jr., J.J. Rehr, Geochim. Cosmochim. Acta 60 (1996) 3023–3038.
[45] Y. Iwasawa, Adv. Catal. 35 (1987) 187–264.
[46] L. Ferretto, A. Glisenti, Chem. Mater. 15 (2003) 1181–1188.
[47] S.E. Collins, M.A. Baltanás, A.L. Bonivardi, J. Catal. 226 (2004) 410–421.
[48] A.H. Nielsen, H.H. Nielsen, Phys. Rev. 48 (1935) 864–867.
[49] P. Bergamaschi, M. Schupp, G.W. Harris, Appl. Opt. 33 (1994) 7704–7716.
[50] M.A.H. Smith, D.C. Benner, A. Predoi-Cross, V.M. Devi, J. Quant. Spectrosc. Radiat. Transf. 112 (2011) 952–968.
[51] C. Wang, R.L. Thomson, J. Baltrus, C. Matranga, J. Phys. Chem. Lett. 1 (2010) 48–53.
[52] S. Linic, U. Aslam, C. Boerigter, M. Morabito, Nat. Mater. 14 (2015) 567–576.
[53] W. Hou, S.B. Cronin, Adv. Funct. Mater. 23 (2013) 1612–1619.
[54] F. Sastre, A.V. Puga, L. Liu, A. Corma, H. García, J. Am. Chem. Soc. 136 (2014) 6798–6801.